Molecular Simulation of Thermo-osmotic slip

Raman Ganti,[1] Yawei Liu,[2] and Daan Frenkel[1,*]

[1] *Department of Chemistry, University of Cambridge, Lensfield Road, Cambridge CB2 1EW, UK*
[2] *Beijing University of Chemical Technology, Beijing, P. R. China*

(Dated: June 13, 2017)

Thermo-osmotic slip – the flow induced by a thermal gradient along a surface – is a well-known phenomenon, but curiously there is a lack of robust molecular-simulation techniques to predict its magnitude. Here, we compare three different molecular simulation techniques to compute the thermo-osmotic slip at a simple solid-fluid interface. Although we do not expect the different approaches to be in perfect agreement, we find that the differences are barely significant for a range of different physical conditions, suggesting that practical molecular simulations of thermo-osmotic slip are feasible.

Thermo-osmosis and thermophoresis are phenomena of great practical interest in the context of non-isothermal hydrodynamics [1, 2], non-equilibrium thermodynamics [3], thermophoresis [4–6], and the propulsion of active matter [7]. Thermo-osmosis is usually described phenomenologically as the induced slippage of fluid along an interface, due to an applied temperature gradient. Phoretic motion is driven by the interfacial stresses induced by a temperature gradient in a microscopic boundary region, where the properties of the solvent are influenced by the interactions with the surface (or interface) [4–6].

Clearly, it would be useful to be able to predict thermo-osmotic slip on the basis of a molecular description of the solid-liquid interface. However, in practice this is not simple because much of the existing theoretical framework is couched in terms that assume the validity of a local continuum theory (e.g. Debye-Hückel plus the (Navier-)Stokes equation) and make drastic assumptions about the excess enthalpy density and viscosity near the surface [8]. Yet, crucially, near an interface, a continuum description of the structure or dynamics of a liquid is not allowed. More ominously, the definition of the stress in a liquid is not unique. This non-uniqueness has no effect on the computed value of, say, the liquid-liquid surface tension [9], but it could affect the prediction of phoretic flows, where the *local* value of the stress gradient is what drives the flow. In this paper, we consider this problem and explore novel 'microscopic' methods to predict thermo-osmotic slippage in a simple model system.

The 'classical' approach to predict thermo-osmotic slippage is based on Onsager's reciprocity relations (see Ref. [10]). These relations have previously been used in molecular simulations to compute diffusio-osmotic slip [2]. Derjaguin [11] used Onsager's Linear Non-Equilibrium Thermodynamics (LNET) approach to derive an expression for thermo-osmotic slip. His approach exploits the relation between the flow caused by a temperature gradient and the excess heat flux due to hydrodynamic flow, resulting in the following equation:

$$v_s = -\frac{2}{\eta}\int_0^\infty \mathrm{d}z\, z\Delta h(z)\frac{\nabla T}{T}, \tag{1}$$

where $\Delta h(z)$ is the excess enthalpy density at a height z above the surface and η is the viscosity. The difficulty with this expression is that there is some ambiguity in the microscopic definition of the local excess enthalpy $\Delta h(z)$, a quantity that is also not easy to probe in experiments [4].

The key motivation for our work is that while a continuum approximation to Eq (1) may be sufficient for interaction lengths on the order of tens of nanometers, it does not work for atomic or molecular liquids that do not contain free charges. Rather, the excess enthalpy density $\Delta h(z)$ is a function of the solvent polarity [12], liquid structure in the boundary layer [8], temperature, and pressure. Additionally, the viscosity η can vary dramatically near a (structured) surface. Our approach circumvents all these issues: we argue that the numerical tools that we use can be applied to realistic models that cannot be described using continuum approaches.

To place the various descriptions of thermo-osmotic slip in a broader context, we first consider the classical thermodynamic approach to the problem, based on the assumption of Local Thermal Equilibrium (LTE). We note that neither temperature gradients nor, for that matter, chemical potential gradients can exert a net force on a fluid element in a bulk liquid. Mechanical forces in liquids can only be caused by body forces such as gravity, or by pressure gradients. If temperature gradients cause flow near a surface, it is only because a local pressure gradient is induced. To clarify this, we first consider the thermodynamics of the problem. Consider a temperature gradient $+x$ direction parallel to a hard wall; the z coordinate measures distance per-

pendicular to the wall. Dividing the Gibbs-Duhem relation for an n-component mixture by V and differentiating with respect to x gives

$$\frac{\partial P}{\partial x} = \left(\sum_{i=1}^{n} \rho_i \frac{\partial \mu_i}{\partial T} + \frac{S}{V} \right) \frac{\partial T}{\partial x}, \tag{2}$$

where ρ_i is the number density of species i. The Gibbs-Duhem equation makes use of the fact that the system is homogeneous. A stratified system in equilibrium, is homogeneous in the directions parallel to the stratification, but not perpendicular to it. Hence, here and in what follows, the 'pressure' P refers to a component of the pressure tensor parallel to the surface (e.g. P_{xx}). In the bulk, the pressure is equalised quickly and the fluid reaches hydrostatic equilibrium. Since the bulk pressure is constant, Eq (2) reduces to

$$\left(\frac{\partial \mu_i}{\partial T} \right)_P = -s_i^B \tag{3}$$

using $S = \sum_i N_i s_i$, where s_i is the specific entropy of species i and the superscript B denotes a bulk quantity. At a position z above the surface, the pressure gradient remains. Assuming that there are no gradients of μ_i and T perpendicular to the surface, Eq (3) can be substituted into Eq (2) to give

$$\frac{\partial P(z)}{\partial x} = \left(-\sum_{i=1}^{n} \rho_i(z) s_i^B + \sum_{i=1}^{n} \rho_i(z) s_i(z) \right) \frac{\partial T}{\partial x}. \tag{4}$$

Eq (4) can be simplified by noting that the expression in brackets is the difference between the specific entropy at position z and the bulk specific entropy. Since μ_i and T do not depend on z, $\mu_i = h_i - T s_i$ can be used to rewrite Eq (4) as

$$\frac{\partial P(z)}{\partial x} = \left(\frac{\sum_{i=1}^{n} \rho_i(z)[h_i(z) - h_i^B]}{T} \right) \frac{\partial T}{\partial x} \tag{5}$$

$$= \left(\frac{\Delta h(z)}{T} \right) \frac{\partial T}{\partial x}, \tag{6}$$

where $\Delta h(z)$ is the excess enthalpy density at a distance z from the surface. To compute the flow velocity, we integrate the expression for the pressure gradient using the linearised (Navier-)Stokes equation giving

$$v_s = -\frac{1}{\eta} \int_0^\infty \mathrm{d}z \, z \left(\frac{\Delta h(z)}{T} \right) \frac{\partial T}{\partial x}. \tag{7}$$

This is equivalent to Eq (1) apart from a factor of 2. The factor of 2 in Derjaguin's result arises from his missing a factor of 1/2 in his expression for Poiseuille flow [11].

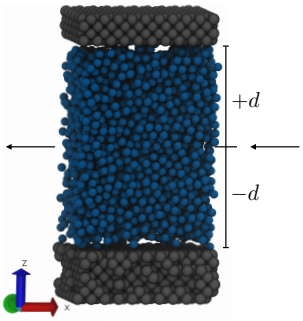

FIG. 1: Atomic fluid (blue) interacting with solid walls (grey) in a slit pore. $2d$ is the gap width.

To relate our LTE expression to Derjaguin's LNET approach, consider the slit pore as depicted in Fig. 1. A pressure and temperature gradient is maintained across the slit. Fluid flows in the $-x$ direction as depicted by the arrows. For a one-component fluid, the resulting phenomenological equations are

$$v_x = -\beta_{11} \nabla P - \beta_{12} \frac{\nabla T}{T} \tag{8}$$

$$Q_x = -\beta_{21} \nabla P - \beta_{22} \frac{\nabla T}{T}. \tag{9}$$

where v_x is the fluid velocity (m/s) and Q_x is the heat flux $(J/(m^2 \cdot s))$. Following Derjaguin [11], by considering the isothermal heat flux across the pore, β_{21} can be expressed as

$$\beta_{21} = -\left(\frac{Q_x - h^B v_x}{\nabla P} \right)_T. \tag{10}$$

β_{21} defined here is conventionally known as the 'mechano-caloric' coefficient. Similarly, by considering the isobaric mass flux in Eq (8), we can write

$$\beta_{12} = -\left(\frac{v_x}{(\nabla T/T)} \right)_P. \tag{11}$$

Assuming that the hydrodynamic flow in Eq (10) is linear in the boundary layer $v_x(z) = -dz \nabla P/\eta$ and substituting Eq (7) for v_x in Eq (11) immediately shows $\beta_{12} = \beta_{21}$ as expected. This provides the link between our LTE and Derjaguin's LNET approach.

The usual definition of the 'slip' velocity is the extrapolated velocity at the interface, where the fluid density approaches zero. For a thin boundary layer, the slip velocity is equal to the fluid velocity in the bulk just outside the boundary layer. β_{12} in Eq (11) is the 'thermo-osmosis' coefficient.

Of course, the analytical theory given by Eqs (5)-(7) is inappropriate for a molecular description of

slip. The viscosity η is not constant near the interface. To avoid making such continuum assumptions, we compute thermo-osmotic slip, using a mechanical route, i.e. by computing the force on a volume element directly from the gradient of the microscopic stress. Such an approach could be problematic due to the non-uniqueness of the definition of the microscopic stress. Han [13] postulated a similar approach, however, did not validate his results.

We start with the relation between the stress gradient and $f_x(z)$ the force per unit volume on a fluid element at a distance z from the surface. Rather than computing the stress gradient in a non-equilibrium simulation, we use the fact that P_{xx} depends on x, only through T. Hence,

$$f_x(z) = -\left(\frac{P_{xx}^{eq,T_2}(x,z) - P_{xx}^{eq,T_1}(x,z)}{T_2 - T_1}\right)\left(\frac{\partial T}{\partial x}\right), \tag{12}$$

where the superscript eq denotes equilibrium calculations that are both carried out at the same bulk pressure. With this method, $\Delta P/\Delta T$ is determined, and for any $\partial T/\partial x$, $f_x(z)$ can be computed via Eq (12). The thermo-osmotic force per particle $f_x^P(z) = f_x(z)/\rho_{ave}(z)$ where $\rho_{ave}(z) = (\rho(T_1,z) + \rho(T_2,z))/2$. To compute the thermo-osmotic flow, we carry out a second simulation at the average temperature $T_{ave} = (T_1+T_2)/2$, where we apply the local body force $f_x^P(z)$ to fluid particles. The resulting slip velocity and therefore β_{12} can then be computed.

The calculation as described above is complicated by the fact that the pressure tensor in an inhomogeneous fluid is not unique [14, 15]. Irving and Kirkwood (IK) [16] proposed an expression by integrating the total momentum flux acting across a virtual surface element. This approach gives the appropriate mechanical force balance normal to the interface. However, as argued by Schofield and Henderson [9], the definition of the pressure tensor is not unique since any term with a vanishing divergence can be added without changing the momentum flux. All common definitions do, however, yield the correct surface tension.

In a simulation, we need to know the thermo-osmotic force acting on atoms, as opposed to the force on the fictitious surface of a volume element. This would suggest that the atom-based virial (V) expression for pressure might be preferable.

In order to determine if the choice of the pressure affects the computed thermo-osmosis coefficient, we computed P_{xx} in Eq (12) using both the V and IK expressions. The V pressure is given by [17]

$$P_{xx}^V(z) = \langle\rho(z)\rangle k_B T - \frac{1}{2V(z)}\left\langle \sum_i^{N(z)} \sum_{j\neq i} \frac{x_{ij}^2}{r_{ij}}\phi'(r_{ij})\right\rangle. \tag{13}$$

where r_{ij} is the distance between atoms i and j, x_{ij} is the distance in x, $\phi(r_{ij})$ is the interaction potential between the atoms, $V(z)$ and $N(z)$ are the bin volume and number of atoms in the bin at position z. The IK pressure is computed using [18]

$$P_{xx}^{IK}(z) = \langle\rho(z)\rangle k_B T - \frac{1}{2A}\left\langle \sum_i^N \sum_{j\neq i} \frac{x_{ij}^2}{r_{ij}} \frac{\phi'(r_{ij})}{|z_{ij}|}\Theta\left(\frac{z-z_i}{z_{ij}}\right)\Theta\left(\frac{z_j-z}{z_{ij}}\right)\right\rangle. \tag{14}$$

In addition to these 'mechanical' expressions for the thermo-osmotic force, consider the right-hand side of Eq (5). We express the local specific enthalpy as

$$h(z) = u(z) + \frac{P_{xx}^V(z)}{\rho(z)}, \tag{15}$$

where u is the specific internal energy. In Eq (15), we have made explicit that the pressure that enters into the expression for the local enthalpy must be the component that is parallel to the surface, as argued below Eq (2). The body force on a fluid element at a height z above the surface is then given by

$$f_x(z) = -\frac{\rho(z)(h(z) - h^B)}{T}\left(\frac{\partial T}{\partial x}\right). \tag{16}$$

Eq (16) can be computed in a simulation thermostatted at T_{ave} and applied as a body force in the same vein as Eq (12).

We compare the above calculations of the slip coefficient with the result for β_{21} that follows from Derjaguin's approach based on the Onsager reciprocity relations. In this case, a uniform pressure gradient represented by a body force is applied during a simulation at T_{ave}. β_{21} is computed via Eq (10) (see Supplemental Material S2). The mechanical and LTE approaches for computing β_{12} and the 'Derjaguin' method for computing β_{21} should be equivalent if the temperature and pressure gradients are small enough to ensure that the resulting response is linear. Thus, we also include in this paper the first molecular simulation of the 'mechano-caloric' effect.

All Molecular Dynamics simulations reported here were performed using the LAMMPS package [19]. The simulation setup is depicted in Fig. 1. The system consists of $N = 2640$ fluid atoms interacting

with other fluid atoms and solid atoms via a truncated and shifted Lennard-Jones potential.

$$V_{\text{trunc}}(r) = \begin{cases} 4\epsilon\left[\left(\frac{\sigma}{r}\right)^{12} - \left(\frac{\sigma}{r}\right)^{6}\right] - V(r_c) & r \le r_c \\ 0 & r > r_c. \end{cases} \tag{17}$$

where $r_c = 4\sigma$, $\sigma_{\text{fluid-fluid}} = \sigma_{\text{solid-fluid}} = \sigma$ and $\epsilon_{\text{fluid-fluid}} = \epsilon$. Two different wall-fluid interactions were investigated: a less attractive Lennard-Jones potential where $\epsilon_{\text{solid-fluid}} = 0.55\epsilon$ and a purely repulsive Weeks-Chandler-Andersen potential [20] such that $r_c = 2^{1/6}\sigma$ for solid-fluid interactions. Solid atoms are bonded via harmonic springs to their nearest neighbors in an fcc lattice of density $0.9\sigma^{-3}$. The stiffness $k_{bond} = 5000\epsilon/\sigma^2$ and rest length is 1.1626σ. All computed quantities are expressed in Lennard-Jones reduced units.

NVT dynamics with a time step $\Delta t = 0.001\tau$ were run to equilibrate the system. This was accomplished using a Nosé-Hoover thermostat for $100,000$ MD steps. For an additional $100,000$ steps, the system was barostatted at P≈ 0.122 by applying a downward force to the top wall atoms.

Using the pressure profiles (see Supplemental Material: Figs. S1(a,b)), $\Delta P_{xx}(z)/\Delta T$ was computed for the three temperatures shown in Figs. 2(a) and 2(b). Encouragingly, the choice of the pressure tensor makes no significant difference to the measured response.

At constant temperature, T_{ave}, the specific kinetic energy is uniform everywhere and therefore computed by dividing the total average kinetic energy by the number of atoms. For the same temperatures, the specific potential energy profiles were spatially averaged in z. Using the profiles of P_{xx} (Fig. S1(a)) and density profiles (Fig. S1(c)), $\Delta h(z)/T$ was computed via Eqs (15) and (16) and shown in Fig. 2(c).

We note that the V and IK expressions (Figs. 2(a), 2(b)) and the LTE quantity Fig. 2(c) show similar qualitative behavior. The body force vanishes in the bulk and the profiles flatten and shift outward as the temperature is increased.

The body force per particle $f_x^P(z)$ can be computed by dividing the profiles in Figs. 2(a-c) by $\rho(z)$ (Fig. S1(c)) and multiplying by a sufficiently small gradient e.g. $\partial T/\partial x = 0.0005$ for WCA wall-fluid interactions. To compute slip, non-equilibrium simulations were carried out by applying these forces to the equilibrated systems at the appropriate temperatures. To obtain reasonable statistics, forces were applied for 10^8 steps until the fluid approached a steady velocity. The slip was then computed for an additional 2×10^8 steps.

Figs. 3(a,c) show calculations of the slip velocity.

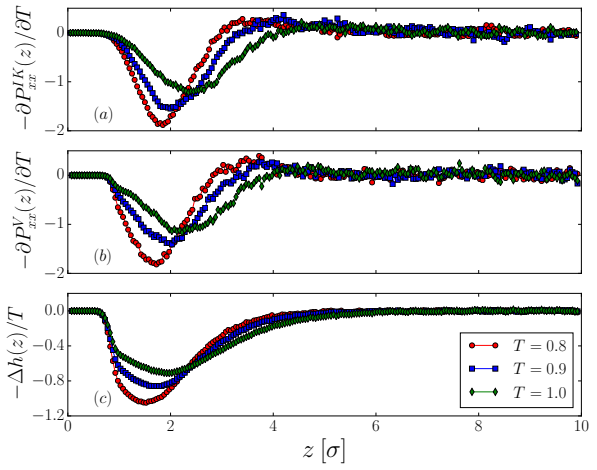

FIG. 2: $-\Delta P_{xx}(z)/\Delta T$ $[k_B/\sigma^3]$ computed using the (a) IK and (b) V pressure tensor e.g. the profile for $T = 0.8$ is computed by taking the difference in P_{xx} at $T = 0.85$ and 0.75 and dividing by $\Delta T = 0.1$. (c) WCA wall-fluid interactions significantly exclude volume and thereby create a large enthalpy difference at the surface. The solid wall is located at $z \sim 0$.

Interestingly, although the mechanical and LTE approaches give different force profiles (Fig. 2), they predict the same velocity far away from the surface. The flow profile computed at $T = 0.9$ (Fig. 3(b)) shows that for WCA wall interactions the velocity decreases monotonically, indicating that the viscosity close to the surface is constant. For less attractive Lennard-Jones (Fig. 3(d)), the viscosity and forces are clearly not constant showing significant departure from (Navier-)Stokes and Derjaguin's result (Eq (1)).

To compare our stress gradient and LTE approaches with Derjaguin's method (see Supplemental Material S2), β_{12} was computed via Eq (11) using the slip calculations shown in Figs. 3(a,c). Fig. 4 shows a comparison of all three methods. For the range of temperatures, there appears to be reasonable agreement. For $T \sim 96 - 120$ K in Argon units, the thermo-osmosis coefficient ranges from $0.85 - 3.8 \times 10^{-8}\text{m}^2/\text{s}$ for less attractive Lennard-Jones and $4.2 - 5.6 \times 10^{-6}\text{m}^2/\text{s}$ for WCA walls.

As expected, the slip velocities for solely repulsive wall-fluid interactions are considerably larger than those for interactions with an attractive component. Furthermore, both cases demonstrate an approximately linear dependence of the thermo-osmosis coefficient with respect to temperature.

In addition to the methods described above, we

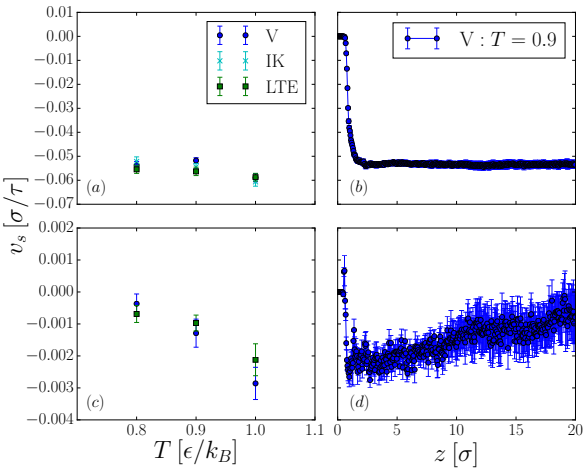

FIG. 3: Calculations of the slip velocity and flow profile for different wall-fluid interactions: (a,b) WCA at $\nabla T = 0.0005$ and (c,d) Lennard-Jones ($\epsilon_{wf} = 0.55\epsilon$) at $\nabla T = 0.003$.

also attempted to compute β_{21} using linear-response theory [21]. However, no reliable results were obtained as the statistical noise overwhelmed the signal.

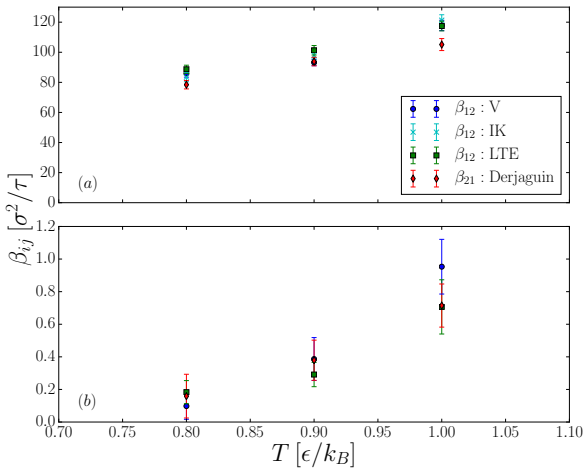

FIG. 4: Comparison of Onsager reciprocal relations, β_{12} computed via our 'stress gradient' (circles, crosses) and LTE (squares) approaches and β_{21} calculated by following Derjaguin's LNET method (diamonds). Thermo-osmosis coefficients are computed for (a) WCA ($\nabla T = 0.0005$, $\nabla P = 0.00004$) and (b) Lennard-Jones ($\nabla T = 0.003$, $\nabla P = 0.0005$) interactions.

Previous molecular simulation studies of thermal transport have dealt with the Soret coefficient of atomic species [22][23]. One cannot directly compare the Soret coefficient S_T with our computed values of the thermo-osmosis coefficient β_{12} since the separation between excess and bulk enthalpy density becomes meaningless if all particles have the same size. As a rough comparison, given that $S_T = (\beta_{12}/T)/D_{Ar}$, taking the average of our computed values of β_{12} for $T = 0.8$ and 0.9 and using $D_{Ar} \simeq 2.47 \times 10^{-5}$ cm^{2}s^{-1} as reported in [23], we compute $S_T \sim 0.047$ K^{-1}, which is the same order of magnitude as $S_T \sim 0.014$ K^{-1} at $T = 0.85$ reported by [23].

In summary, we have considered three different methods to compute thermo-osmotic slip on the basis of molecular simulations. The first approach is based on a computation of the thermally-induced stress gradient method, computed using equilibrium simulations and then represented as a body force in non-equilibrium simulations. We find no evidence that different choices for the pressure tensor lead to different results. In the second approach, we compute the excess enthalpy density near the wall and use a local-thermodynamics formalism to derive the body force acting on the fluid. These methods do not assume that macroscopic thermodynamics or hydrodynamics holds close to an interface. The final approach is based on Onsager's reciprocal relations, which allow us to derive thermo-osmotic slip from the excess heat flux due to a pressure gradient.

The key results are encouraging and surprising: for certain wall-fluid interactions, the thermo-osmotic flow profile does not monotonically depend on the distance from the surface, indicating that the viscosity and forces near the surface are not constant. Furthermore, we find that all methods yield results for the thermo-osmosis coefficient that do not differ significantly. Hence, choice of the method to compute thermo-osmotic slip seems to be a matter of taste or convenience.

We gratefully acknowledge numerous discussions with Lydéric Bocquet, Mike Cates, Patrick Warren, Ignacio Pagonabarraga and Benjamin Rotenberg. Additionally, we are grateful to Peter Wirnsberger for his help with the error analysis. RG gratefully acknowledges a PhD Grant from the Sackler Fund.

* Corresponding author; df246@cam.ac.uk

[1] J. Morthomas and A. Würger, J. Phys. Condens. Matter **21**, 035103 (2009).

[2] A. Ajdari and L. Bocquet, Phys. Rev. Lett. **96**, 186102 (2006).

[3] J. Dhont, S. Wiegand, S. Duhr, and D. Braun, Langmuir **23**, 1674 (2007).

[4] J. Anderson, Annu. Rev. Fluid Mech. **21**, 61 (1989).

[5] R. Piazza and A. Parola, J. Phys. Condens. Matter **20**, 153102 (2008).

[6] A. Würger, Rep. Prog. Phys. **73**, 126601 (2010).

[7] R. Golestanian, T. Liverpool, and A. Ajdari, New J. Phys. **9**, 126 (2007).

[8] A. Bregulla, A. Würger, K. Günther, M. Mertig, and F. Cichos, Phys. Rev. Lett. **116**, 188303 (2016).

[9] P. Schofield and J. Henderson, Proc. R. Soc. A **379**, 231 (1982).

[10] S. de Groot and P. Mazur, *Non-equilibrium Thermodynamics* (North Holland Publishing, Amsterdam, 1962).

[11] B. Derjaguin, N. Churaev, and V. Muller, *Surface Forces* (Plenum, New York, 1987).

[12] S. A. Putnam and D. G. Cahill, Langmuir **21**, 5317 (2005).

[13] M. Han, J. Colloid Interface Sci. **284**, 339 (2005).

[14] B. Hafskjold and T. Ikeshoji, Phys Rev E Stat Nonlin Soft Matter Phys **66**, 011203 (2002).

[15] J. Rowlinson and B. Widom, *Molecular Theory of Capillarity* (Dover Publications, 2003).

[16] J. Irving and J. Kirkwood, J. Chem. Phys **18**, 817 (1950).

[17] J. Hansen and I. McDonald, *Theory of Simple Liquids* (Elsevier, 1990).

[18] J. Walton, D. Tildesley, J. Rowlinson, and J. Henderson, Mol. Phys. **48**, 1357 (1983).

[19] S. Plimpton, J. Comput. Phys. **117**, 1 (1995).

[20] J. Weeks, D. Chandler, and H. Andersen, J. Chem. Phys **54**, 5237 (1971).

[21] J. Luttinger, Phys. Rev. **135**, A1505 (1964).

[22] F. Römer, Z. Wang, S. Wiegand, and F. Bresme, J. Phys. Chem. B **117**, 8209 (2013).

[23] D. Reith and F. Müller-Plathe, J. Chem. Phys **112**, 2436 (2000).

Supplemental Material: Molecular Simulation of Thermo-osmotic slip

Raman Ganti, Yawei Liu, Daan Frenkel

February 22, 2017

1 Pressure Computation

As discussed in the main text, the molecular definition of pressure is not unique. In order to determine if this non-uniqueness impacts our result, we compute the pressure tensor using both the virial and Irving-Kirkwood expressions. The virial is given by

$$P_{xx}^{Vir}(z) = \langle \rho(z) \rangle k_B T - \frac{1}{V(z)} \left\langle \frac{1}{2} \sum_{i}^{N(z)} \sum_{j \neq i} \frac{x_{ij}^2}{r_{ij}} \phi'(r_{ij}) \right\rangle. \tag{1}$$

Irving-Kirkwood is computed using

$$P_{xx}^{IK}(z) = \langle \rho(z) \rangle k_B T - \frac{1}{2A} \left\langle \sum_{i}^{N} \sum_{j \neq i} \frac{x_{ij}^2}{r_{ij}} \frac{\phi'(r_{ij})}{|z_{ij}|} \Theta\left(\frac{z - z_i}{z_{ij}}\right) \Theta\left(\frac{z_j - z}{z_{ij}}\right) \right\rangle. \tag{2}$$

For a range of temperatures $T \approx 0.75 - 1.05$, the pressure and density profiles were averaged in slabs at constant height for 3×10^7 time-steps for $\Delta t = 0.001\tau$, where $\tau = \sigma(m/\epsilon)^{1/2}$ in Lennard-Jones reduced units. We found that a slab thickness $\mathrm{d}z = 0.05$ gave sufficient resolution. Figures 1a and 1b show the virial and Irving-Kirkwood pressures computed via Eqs (1) and (2) for WCA wall-fluid interactions. As the temperature is increased, the difference between the surface and bulk pressure decreases. In the bulk, all profiles converge to $P \approx 0.122$ as expected.

2 'Derjaguin' Method

As derived in the main text, β_{21}, the ratio of the isothermal excess heat flux to the externally imposed pressure gradient, is given by

$$\beta_{21} = -\left(\frac{Q_x - h^B v_x}{\nabla P}\right)_T. \tag{3}$$

It can be computed by re-expressing Eq (3) as

$$\beta_{21} = \left(\frac{\frac{1}{V}\left[\sum_i^N (p_i^2/2m + \sum_{i<j} \phi_{ij}) v_i^x - 1/2 \sum_{i<j} (x_{ij}^2/r_{ij}) \phi'(r_{ij}) (v_i^x + v_j^x) - \sum_i^N h^B v_i^x\right]}{\nabla P} \right)_T. \tag{4}$$

To compute β_{21}, a uniform pressure gradient was simulated by applying a force per particle $f_x^P(z) = -\nabla P/\rho(z)$ to all fluid atoms. Figure 2a shows the force profile for different values of ∇P at $T = 0.9$. Body forces were applied for 10^8 steps and the excess heat flux as expressed in Eq (4) was computed for 2×10^8 steps. Figure 2b shows calculations of β_{21} for each force profile. For sufficiently small gradients, β_{21} remains constant indicating transport in the linear regime. Within this regime, LNET applies. As the gradient increases, β_{21} increases, indicating entry into a nonlinear regime. In the bulk, the excess heat current should vanish as indicated by $\beta_{21} \approx 0$ while outside of the linear regime $\beta_{21} > 0$.

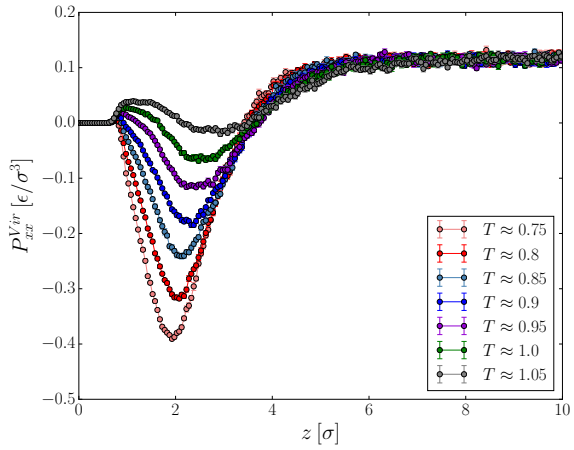

(a)

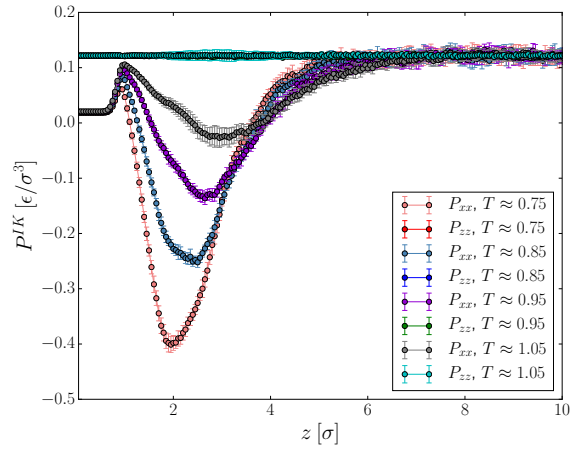

(b)

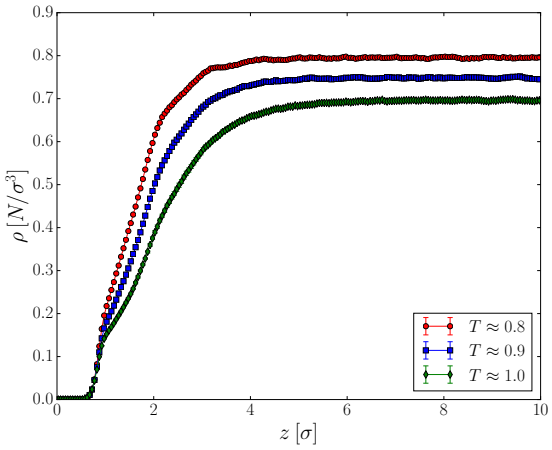

(c)

Figure 1: 1a and 1b show $P_{xx}^{Vir}(z)$ and $P_{xx}^{IK}(z)$ respectively for simulations conducted at different temperatures. P_{zz}^{IK} in 1b remains constant for all T, satisfying mechanical equilibrium normal to the surface. Density profiles for the temperatures of interest are shown in 1c.

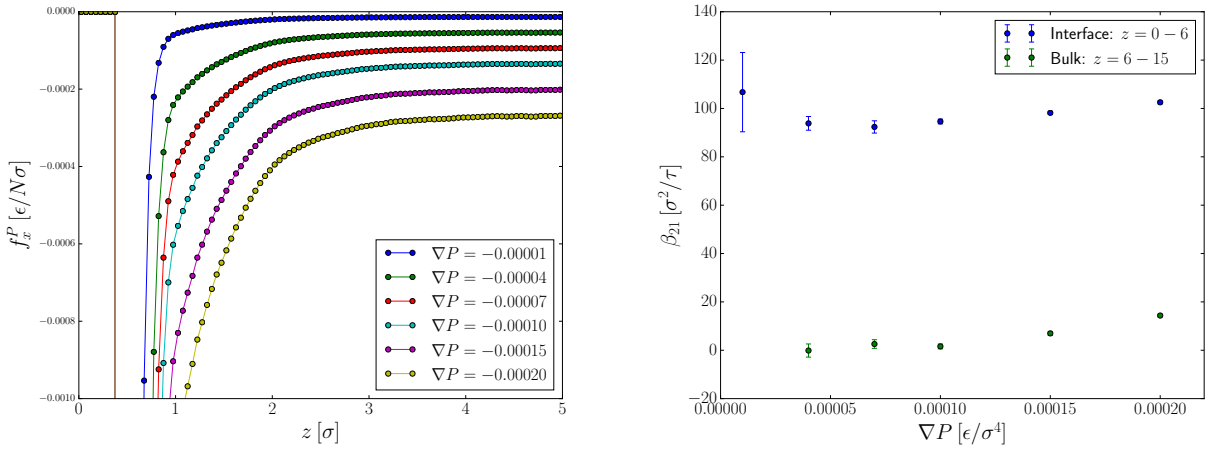

(a) (b)

Figure 2: 2a shows the force per particle that must be applied in order to simulate a uniform ∇P. A range of pressure gradients was tested in separate simulations to determine the extent of the linear regime. The mechano-caloric coefficients β_{21} for these gradients are shown in 2b. Blue dots correspond to integration of the excess heat flux from the wall ($z \approx 0$) into the bulk ($z \approx 6$). In the linear regime, $\beta_{21} \approx 92 - 95$. Green dots correspond to integration of the excess heat flux in the bulk where, as expected, it is approximately zero.